Real-time Identification and Prediction of unsafe zones in extreme events

Industrial disasters such as fires, accidents and explosions etc. result in uncontrolled emission of toxic chemicals and gases in the atmosphere and affect large regions in their vicinity. In order to plan an effective and safe rescue strategy, it is extremely important to collect information about toxic substances present in the affected area and not only identify hazardous regions but also predict the regions that might be at risk.

After an event happens, there is hazardous substance released into the atmosphere that can spread up to a few kilometers in just few minutes [1]. In such scenarios the immediate first responders take action within the first two hours. Hence, the scenario we are considering in this project is focused on flying the drones equipped with gas-sensors around the affected site soon after the event took place. The drones collect gas concentration measurements that are used to identify regions where toxic concentrations are above the safe level and predict the regions that might cross the safe threshold in near future. All these goals must be achieved in real-time and a danger-zone classification of an area up to a few kilometers should be provided to the first responders within the first few hours.

It must be noted that as time passes the size of area where the gas/contaminant has reached gets bigger and bigger. However, this dispersion, that depends on the physical and weather conditions of the area, drastically impacts the distribution of the contaminant in a given spatial region and makes it a very dynamic entity. Therefore, spotting the danger zones in real-time is not a ver challenging task. Furthermore, the limited speed and flight time of the drones strongly limit the amount of information that can be collected from the affected region.

1 System Model

In this project, we focus on the extreme events with single emission source. There are three main system components that define the scenario. Firstly a contaminant/gas plume is released by an industrial source and is mathematically represented by a concentration region above a given threshold. We do not make any assumptions about the plume being in steady state and therefore the concentration values are varying over time. We further assume that the emission happened from an instantaneous source. Instantaneous source e.g explosion releases large amount of contaminant into the environment instantaneously and do not contribute as a source afterwards.

Next, we define a spatial region about which we want to make classification decisions of being safe or not. Since in industrial accidents like fires and explosions, the source location is already known, the spatial region can be easily defined around that source. Along with source location, another piece of information that is easily available is the average wind velocity.

Finally, we have drones equipped with gas sensors. The gas sensors measure the concentration of gas at a given time and location with almost zero sensing range. Along with the limited range, they also have a response time of the order of seconds which poses great challenge since it highly limits the amount of information that can be sampled from the region of interest. Since, the initialization is very critical, it is important to specify from where the drones start their mission. In our scenario, the drones fly together from the point called Ground Station. Also note that the drones are constrained in their resources and have highly limited speed and flight time.

With the constraints imposed by the drones and gas sensors, our end-goal is to use these concentration measurements to obtain the Gas Distribution Map (GDM) for current time and predict how it will evolve in future with as high accuracy as possible. These goals would map to classification of regions into safe and danger zones directly when compared against a pre-determined safety threshold.

To achieve these end goals, there are two main objectives that should be met. The first objective is to optimally *use* the drone measurements to estimate the current GDM and predict the next with minimum error. The second objective is to efficiently *choose* the locations to be sampled by drones that maximize the estimation and prediction accuracy while meeting the constraints imposed by the drone resources and sensor capabilities.

While we formulate the problem and design a system to achieve these objectives, there are three key factors that must be satisfied. It should be generalizable, light-weight and able to handle spatiotemporal data.

Firstly, it should be kept in mind that these extreme events can happen in any circumstances. The spread of contaminant gas depends on many factors that are not only beyond our control but also can't be measured. To name a few, these include weather conditions, chemical properties of contaminant gas and topography. This variability that is introduced in these extreme event situations require that our system design is fairly generalizable. It discourages us from adopting solutions that assume the underlying system to follow a certain function or distribution and then try to fit the data to that assumed model.

Secondly, the urgency of the situation and the resources of the drone require that the solution should be light-weight and fast. For instance, we can not afford to run computational fluid flow simulations that not only require high resolution weather and atmospheric data but can take up to days to yield a solution.

Finally, if we observe the entity that we want to estimate i.e the gas concentrations, we see that it is a function of both space and time and we need its characterization over both these independent variables. Also the data we are sampling is a time-stamped concentration data at particular locations. Thus, it is essential that our problem formulation and the final solution should both be able to handle spatiotemporal data.

2 Mathematical Formulation

In this section, we formally state the mathematical description of our system model. Since we require a formulation that is simple and light-weight, can handle spatiotemporal data and is fairly generalizable, we utilize state-space description for our problem.

However, before moving to the actual equations, we first discretize our system in both space and time domain. While ideally we want to have a real-time identification of high-concentration regions with negligible delay, we are bounded by the response time of sensors and the limited speed at which the drones can fly. Also the system that we are trying to identify is a complex system and for reasonable estimates we need sufficient samples before we make classification decisions. All these factors define the length of time windows that we use to specify the frequency of our estimates and predictions. After time discretization, the spatial region of interest is discretized into N points and each point has a corresponding concentration level. Thus, the concentration map at time index n can be expressed as a 2D matrix with rows and columns denoting the Cartesian coordinates and the entries of matrices represent the concentration value. The matrix columns can also be stacked to obtain a 1D vector of length N. Since, we formulate our problem in State space setup, we adopt the vector representation.

Let $c[n]$ of size $N \times 1$ represent the concentration map at time n. Then the evolution of concentration map can be expressed as,

$$c[n+1] = Ac[n] + n \tag{1}$$

where A is an $N \times N$ transition matrix and n represents the $N \times 1$ process noise vector. The concentration map at time $(n+1)$ is a sum of weighted and additive combination of previous map and a process noise term. The process noise accounts for the uncertainty we have about this model and the transition matrix. In addition to the transition model, we have the measurement model,

$$y[n] = Hc[n] + w \tag{2}$$

The dimensions of $y[n]$ and w are $M \times 1$ and represent the measurement and sensor noise vector respectively. The matrix H of dimensions $M \times N$ is an indicator matrix with ones for locations that are being sampled. Both process and measurement noise are modeled as Gaussian processes with zero mean and covariance matrices Q and R. Please note that measurement noise is not that critical and the main challenges are associated with using those measurements for estimation.

3 Identification of danger zones

With the system model provided in previous section, there are two main objectives that need to be achieved. Firstly, using a given set of noisy measurements of a few states of the system determined by the indicator matrix H, an estimate of $c[n]$ and a prediction of $c[n+1]$ is required. Secondly, the indicator matrix H has to be designed and updated to adaptively choose sampling locations that maximize the estimation accuracy. These two objectives map to two modules that operate recursively in a feedback loop. In this section, we design the estimation and prediction module that takes care of the first objective.

It should be noted that our objective is not limited to using the measurements to estimate the current GDM only. In fact in addition to estimation we predict the evolution of that map too. Thus, it is important that we integrate these prediction with the actual measurements taken at later time to get an optimal estimate of the GDM. Leveraging both measurements and predictions is also very crucial to overcome the limitations imposed by extremely small amount of measurements. Our system is an underdetermined system where our measurements are far less than the unknowns we are trying to estimate. Hence, estimation methods like least squares that utilize current measurements only, i.e are based on (2) only, are not feasible for estimating the complex GDM snapshots from few noisy measurements taken from the same snapshot.

In order to combine the noisy measurements with the predictions in an optimal way, we use Kalman filter. Kalman filter is well-suited for our problem because it is a light-weight, efficient and recursive method that doesn't add computational burden on the drones and provides real-time estimate of GDMs. Furthermore, it is a flexible method with design parameters that can be tweaked according to the mission scenario. For example, based on the quality of gas sensors, the noise variances can be adjusted.

While the noise variances allow us to adjust the Kalman filter according to the mission scenario, the transition matrix A is a crucial element that is required and that determines the accuracy of our estimates. The transition matrix that allows us to extrapolate our estimates in time and gives us the ability to predict is the key element in any strategy that aims to integrate the predictions with the measurements for high-accuracy estimation.

Before we use this model for identifying unsafe zones and predict regions at risk, the most crucial part of the system i.e the transition matrix needs to be estimated. In the next section, we provide two methods that first define a method to construct A and then leverage the measurements to get an estimate of A.

3.1 System Identification

In order to obtain an accurate estimate of GDM $c[n]$ from noisy measurements, the transition matrix A is required. Since the matrix A is also an unknown, we need to estimate it from the drone measurements. Learning the state-space system matrices, such as A, from measurements is also known as system identification.

Our objective in this section is to find methods that can learn the transition matrix of a complex system that has a high dependency on several parameters that can neither be measured nor be controlled. This introduces high variability in the system and we require our methods to be robust to this variability. To achieve this, the learning strategy should rely heavily on the actual measurements instead of assumed models or distributions. However, for high accuracy, a data-only strategy would demand large amount of diverse measurements. In our scenario, the amount of data that can be sampled is bounded by the limited drone resources. In this case, the physical principles of gas dispersion can be exploited in such a way that the generalizability of the system is not compromised too much. Thus, we provide two methods for estimating the transition matrix.

The first one is a *purely* Data-driven system identification method that uses the time-series measurements only and do not require any additional information about the source or weather. The second method, which we call a Model-based approach, integrates the

concentration measurements with the domain knowledge and leverages the information we have about the source. Please note that integration of domain knowledge provides advantage in terms of having an additional information but it also adds a bias.

3.1.1 Purely Data-Driven Method

Matrix-Pencil method is a tool for system identification/realization from experimental data.It provides a mechanism to construct transition matrix A from noisy measurements. This method is simple and light-weight that makes it very suitable for on-drone implementation. It can handle noisy spatiotemporal data and therefore we can easily feed the time-stamped concentration measurements directly to it. It doesn't put any constraints on the form or distribution of A that makes it fairly generalizable.

The method is based on the idea of exploiting the property of pencil and was formally developed in 1990 [2]. Before we explain the method itself, we want to highlight the main principle behind it. As we know from equation (2), the measurements are as a sum of true states and Gaussian noise. Matrix Pencil method aims to construct the noise-free signal from the measurements by exploiting the pencil structure and formulating a generalized eigenvalue problem. The construction of pencil is parameterized by its length and is the only design parameter that impacts the performance at a given SNR. We can imagine the construction of matrix pencils as a moving window across the measurements. Thus, the design space of this method constitutes of only one parameter which is the length of time series data. While larger window provides more information it also acts like a memory. Incorporating too much data from the past can add unnecessary impact of the old measurements that are no longer correlated with the current data. Thus, an upper bound should be set for this parameter.
Now we explain the major steps of the method. Let $y[k] \in \mathcal{R}^M$ represent the measurements taken at discrete time step k. With P as the pencil length, we construct two shifted Hankel matrices as follows,

$$H_0 = \begin{bmatrix} y[0] & y[1] & y[2] & . & . & . & y[L-1] \\ y[1] & y[2] & . & . & . & . & . \\ . & . & . & . & . & . & . \\ . & . & . & . & . & . & . \\ y[P-L-1] & . & . & . & . & . & y[P-1] \end{bmatrix}, H_1 = \begin{bmatrix} y[1] & y[2] & y[3] & . & . & . & y[L] \\ y[1] & y[2] & . & . & . & . & . \\ . & . & . & . & . & . & . \\ . & . & . & . & . & . & . \\ y[P-L] & . & . & . & . & . & y[P] \end{bmatrix} \tag{3}$$

where the size of each matrix is $M(P-L) \times L$. In the next step, we decompose the H_0 using singular value decomposition,

$$H_0 = USV' \tag{4}$$

Where U and V are unitary matrices containing the left and right eigenvectors of H_0 and S is diagonal matrix of size $M(P-L) \times L$ with eigenvalues stacked along its diagonal. It must be noted that the SVD factorization allows us to reduce the order of the system to $n < min(M(P-L), L)$ by choosing n largest eigenvalues and corresponding eigenvectors. However, as mentioned earlier, our measurements are already very limited and do not constitute a computational burden by any means. Proceeding to the final step, the transition

matrix A is constructed using (3) and (4),

$$A = S^{-1/2} U' H_1 V S^{-1/2} \tag{5}$$

It can be observed from (5) that in order to construct a system matrix of size $N \times N$, the rank of Hankel matrices should be at least N which further puts a lower bound on the window length parameter, $min(M(P-L), L) \geq N$. This condition incurs an initial overhead on the system and the drones need to sample for N time instances instances in the initial phase before the first estimate of transition matrix can be obtained. This overhead can be extremely long and might drain the entire drone battery if N is too large. A simple solution that can be adopted in such scenario is obtaining a lower-order state-space solution and extrapolating them in space using a standard method like Gaussian kernel extrapolation. This limitation also reflects that while this method can extrapolate the data in time domain, it has limited ability to estimate unmeasured system states using data from other locations.

3.1.2 Model-based Approach

In this section, we propose an alternate method of learning the transition matrix by integrating the domain knowledge of the system with the measurements. The dispersion mechanism that explains how gases are transported in the environment is a valuable source of knowledge that is expressed in the form of a partial differential equation called the transport equation. We derive a parametric model for the transition matrix A by utilizing the transport equation and the information about source location and wind velocity. This allows us to express A as a function of only one parameter which is diffusion coefficient D. It is further shown that only two set of measurements at different time stamps are required to estimate D. Compared to purely data-driven method that requires N set of measurements, this method can provide a much quicker solution. As would be shown later in this section, the final formulation derived from the transport equation consists of matrices that take care of the numerical solution (i.e discretization and interpolation). The parameters of the numerical scheme i.e discretization resolution and choice of interpolation functions define the design space of this method.

When a contaminant or gas is released in the environment by a point source, there are two main physical phenomenon responsible for its spread. The first one is diffusion which is caused by the inherent Brownian motion of particles and is determined by the physical characteristics of released contaminant/gas itself, surrounding medium which is air and the atmospheric conditions such as temperature and humidity. The second phenomenon which is mainly responsible for long distance spread in short time spans is advection and is caused by the wind. Essentially, it quantifies the tendency of wind to carry the contaminant away from the source. Together they can be expressed mathematically for incompressible flows by the advection-diffusion Partial Differential Equation (PDE) or more commonly known as Transport equation,

$$\frac{\partial c}{\partial t} = D\nabla^2 c - \mathbf{v} \cdot \nabla c + s \tag{6}$$

where c represents the concentration field which is a function of both space $[x, y, z]$ and time t. D and $\mathbf{v}$ represent the diffusion and wind field vector respectively and s represents the source term. The equation, based on the conservation principles, explains that the variation

in concentration field in any region is equal to the flux across the region plus the source term. The flux is composed of diffusive flux represented by the first term on the right side of the equation and the advective flux caused by the wind and is shown by the term next to it. Finally the source term includes both release sources that introduce the contaminant in the environment and the sinks such as chemical reactions that might be responsible for removal of contaminant from the environment. Since, it is very hard to even detect if such reactions are happening let alone measuring their parameters, we focus on the source release term only.

As the transport equation characterizes the dispersion of contaminant/gas, it also provides information about the evolution of concentration map in spatial and temporal domain. This evolution is what we need to characterize the transition matrix. Since the transport PDE is parametrized by the diffision coefficient and wind field, we can utilize this PDE to express the transition matrix A in form of a parametrized model that needs information about diffusion and wind only.

In order to achieve this objective we need a solution of transport PDE. However, a closed form solution of (6) do not exist. There are some solutions derived under ideal conditions however, we do not explore that direction because they compromise the generalizability of our solution. We have no control over the atmospheric and weather conditions of the region where the event happens and therefore it would be infeasible to deploy these simple solutions that are derived under special conditions. Thus, we explore the numerical solution of the transport PDE.

In order to obtain the numerical solution of the system, there are two domains that need to be discretized. Discretization is needed not only for the numerical solution of (6) but also because the state-space formulation (1) is in discrete domain. Hence, to obtain the discrete-domain transition matrix, we need to discretize both space and time. For spatial domain with complex geometries, simple scheme like finite difference are inefficient and therefore we use the well-established and efficient finite element method (FEM). FEM also allows choice of higher order interpolation functions that provides better accuracy than Finite-difference method.

The main principle of FEM is to divide the region of interest into small elements defined by their nodes and seeking a solution for each node that satisfies the required properties. The field inside the elements is obtained by performing polynomial interpolation using the values at corresponding nodes. Thus, the design parameters of this scheme are the number of nodes, element geometry and interpolation functions also known as shape functions. Please note that approximation error introduced by this discretization is dependent on the both, the number of nodes and the order of the interpolation function. Higher number of nodes are particularly critical for accurate solutions.

After discretizing the spatial domain into N smaller regions that we call elements, we choose the interpolation functions for each element $i \in \{1, 2, 3, ...N\}$ and denote them by S_i. Now with these design choices, FEM is applied to (6) and a set of algebraic equations that can be expressed through matrix multiplication are obtained through Galerkin method [3].

$$\mathbf{M}\frac{\partial c}{\partial t} = \mathbf{K}c + \mathbf{U}c + \mathbf{f} \tag{7}$$

where,

$$\mathbf{M} = MassMatrix = \sum_{e=1}^{N} \mathbf{M^e}, \;\; M^e_{j,k} = \int_{\Omega_e} S_i S_j d\Omega \tag{8a}$$

$$\mathbf{K} = Diffusion\ Matrix = \sum_{e=1}^{N} \mathbf{K^e}, \;\; K^e_{j,k} = -\int_{\Omega_e} \nabla S_i \cdot D \nabla S_j d\Omega \tag{8b}$$

$$\mathbf{U} = Avection\ Matrix = \sum_{e=1}^{N} \mathbf{U^e}, \;\; U^e_{j,k} = -\int_{\Omega_e} S_i \mathbf{v} \cdot \nabla S_j d\Omega \tag{8c}$$

$$\mathbf{f} = source\ vector = \sum_{e=1}^{N} \mathbf{f^e}, \;\; f^e_i = \int_{\Omega_e} s * S_i d\Omega \tag{8d}$$

Now let's walk through this complex discretized version of transport equation (6). Just like the original PDE, the variation in concentration field on the left hand side of the equation is equal to the sum of discretized flux terms and source vector represented by $\mathbf{f}$. However, the concentration variation term is being multipled by mass matrix $\mathbf{M}$. If we take a closer look at (8a), we observe that mass matrix is the sum of the impact of all elements i.e $\mathbf{M^e}$. Now $\mathbf{M^e}$ is accounting for the contribution e^{th} element is having on all the other $N-1$ elements and is itself an $N \times N$ matrix. Thus, the mass matrix, which is also a symmetric matrix, is responsible for the elements' connectivity and numerical interpolation between those elements making it a completely known parameter in our application.

Moving to the opposite side of equation, the first term represents the diffusive flux and $\mathbf{K}$ denotes the diffusion matrix. Observing the formulation in (8b), we see that $\mathbf{K}$ takes care of the impact of diffusion in the numerical solution and therefore we only require diffusivity coefficient to compute this matrix. Diffusivity coefficient is a physical characteristic of the gas /contaminat and the air around it in which it is diffusing. If we assume that diffusion coefficient is time-invariant and homogeneous i.e it doesn't change in space, then only one parameter needs to be estimated to compute $\mathbf{K}$. The next term is the advective flux and advection matrix $\mathbf{U}$ is computed in a similar way except that it is parametrized by wind velocity. Again assuming that wind velocity is not changing much over space and time, $\mathbf{U}$ can be computed using the average wind velocity.

Please note that all the above matrices are of size $N \times N$. The integration operator can be solved by any standard numerical integration scheme. In our simulations we use Gauss quadrature method for solving the integrals. After completing spatial discretization, we move to temporal domain and replace the time derivative with a difference,

$$\mathbf{M}(\frac{c_{n+1} - c_n}{\Delta t}) + (\mathbf{K} + \mathbf{U})(\theta c_{n+1} + (1-\theta)c_n) = \mathbf{f} \tag{9}$$

where, $\theta \in \{0, 1/2, 2/3, 1\}$

Now considering an instantaneous source, the source term exists only for the time when there is a release, say at $n = 0$, and vanishes afterwards. Furthermore, assuming that the diffusivity coefficient D is constant over space and time, we can express the above equation for the time $n > 0$,

$$c[n+1] = [(\mathbf{M} + \theta * dt * (\mathbf{U} + D * \tilde{\mathbf{K}}))^{-1}(\mathbf{M} - (1-\theta) * dt * (\mathbf{U} + D * \tilde{\mathbf{K}}))]c[n] \tag{10}$$

where, $\tilde{\mathbf{K}} = \sum_{e=1}^{N} \tilde{\mathbf{K}}^{\mathbf{e}}$, $\tilde{K}^{e}_{j,k} = \int_{\Omega_e} \nabla S_i \cdot \nabla S_j d\Omega$ The above equation can expressed in a cleaner notation as follows,

$$c[n+1] = A(D) * c[n] \tag{11}$$

where $c[n+1]$ and $c[n]$ represent the concentration maps at time index $(n+1)$ and n respectively. The parametrized transition matrix A can be expressed as,

$$A(D) = (\mathbf{M} + \theta * dt * (\mathbf{U} + D * \tilde{\mathbf{K}}))^{-1}(\mathbf{M} - (1-\theta) * dt * (\mathbf{U} + D * \tilde{\mathbf{K}})) \tag{12}$$

This representation of transition matrix utilizes the process of diffusion and advection to estimate the evolution of concentration map. Compared to this, the transition matrix derived from pencil method relies on the evolution observed through the measured data only. Also model-based A is parameterized by the diffusivity coefficient D only and therefore, there is only one unknown that needs to be estimated instead of N^2 terms for the whole transition matrix.

Now, we estimate diffusivity coefficient D by integrating the measurements with the physical model given by transport equation. Considering the measurement model,

$$y[n+1] = H * c[n+1] + n \tag{13}$$

where H is MxN indicator matrix. Multiplying both sides of (11) by the indicator matrix and plugging it in (13), we get the following equation,

$$y[n+1] = HA(D) * c[n] + n \tag{14}$$

By using the associative property of multiplication, we can express $A(D) * c[n]$ as $A(D) * y[n]$. Next, we formulate an optimization problem to find D that minimizes the second norm of error,

$$\hat{D} = \arg\min_{D} ||y[n+1] - HA(D) * y[n]||^2 \tag{15}$$

Please note that we only require two set of measurements at the same set of locations and dt apart in order to get an estimate of D. Thus, unlike the matrix pencil method the initial overhead is much smaller that requires N set of measurements initially. Also since the construction of A has dt as an in-built parameter, the measurements are not required to be equally-spaced in time which is a requirement in Matrix-pencil method. However, it must be noted that there is a computational burden associated with computing the inverse of $N \times N$ matrix in (10). There exist more sophisticated methods in literature that allow us to compute an approximate inverse much more efficiently and quickly. These methods can be incorporated in the future work to reduce the computational complexity of the proposed solution.

4 Evaluation

Two methods for estimating the transition matrix were developed in previous section. With the availability of transition matrix estimate, Kalman filter can be successfully deployed to jointly estimate and predict the gas distribution map from a given set of measurements. Now, before we move to the design of flight planning module to optimally choose those measurement locations, it is critical to evaluate the performance of this classification module.

While, the end-to-end perfomance can only obtained after the drone constraints are incorporated through the flight planning module, there are two main reasons to perform an evaluation at this stage. Firstly, compared to fixed sensors, choosing measurement locations dynamically, with reasonable flight time constraints as drones move from one location to another at a limited speed, introduces an additional degradation in performance. Thus, the end-to-end performance would be a coupled effect of both classification and flight planning module and we would not be able to observe the individual impact of classification module and even more importantly compare the two schemes mentioned above in a fair manner. Secondly, the classification module provides a feedback to flight planning module. Therefore, an investigation into the impact of sampling locations on classification performance can be leveraged in the design of flight planning module.

With these two aspects in mind, we conduct different experiments utilizing the Thorney Island Dataset. The dataset is based on controlled experiements conducted to collect concentration data around an instantaneous source after the release of heavy gas.

A brief high-level summary of all the experiments will be added here later after presenting all the results with 4 steps.

4.1 Estimation Accuracy

Issue Reliability of the output decisions i.e identified danger zones is extremely critical since it can risk human lives. The reliability of our proposed solution can be quatified by classification accuracy. While it is known that the average classification accuracy improves as the number of sampling locations increase, It is unclear how it improves. Investigation into this relationship can help provide an upper bound on the achievable reliability.

Research QuestionThus, it is very important to pose this research question about how well can our proposed solution estimate the concentration levels at unsampled locations by utilizing the sampled data. Furthermore, since there are two methods developed in previous section, a comparison is needed. First of all, we need to quantify the gain provided by integration of domain knowledge and additional information about source and wind velocity in the model based approach. Secondly, the integration of transport equation in model-based approach introduces a bias. It is important to find out how does this bias compromise the performance, if it does, especially with increasing number of samples.

4.1.1 Evaluation Methodology

As explained in section 1, generalizability is a key factor in both system design and its evaluation. Since, the physical characteristics of the environment like weather and atmospheric conditions are neither in our control nor they can be completely measured, it is critical

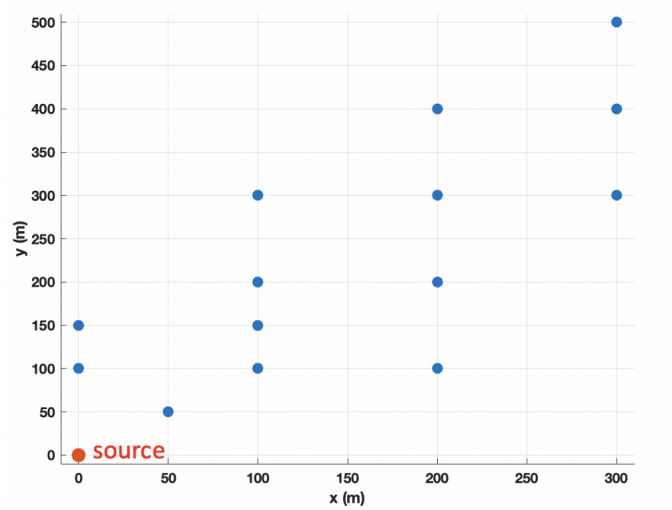

Figure 1: Geometric layout of sensors and source in 2D

to perform an evaluation with field experiment that has those usual characteristic physical conditions. In order to validate the effectiveness of our system, we evaluate it with data collected from a field experiment.

To the best of author's knowledge, this dataset is the only one that provides high resolution concentration data around an instantaneous source. As mentioned in section 1, the temporal scale is a key factor in extreme events. We need the concentration measurements immediately after the incident when the plume is in a transient state. While, there are many other datasets available, they focus on the steady state response and thus the data is recorded on an hourly scale for multiple days. Our time scale requirement is a short time window of few minutes. Moreover, the spatial scale is also significant. We are looking at scenario where the concentration levels are extremely high such that they cross the safety threshold and the area where rescue operation is to be performed by the first responders is in the vicinity of the source. The is an area of radius of few kilometers around the source and therefore datasets that collected for air pollution over the scale of towns and cities are not useful for us.

The dataset contains concentration measurements at fixed locations with sampling frequency of around 1 hertz along with the source location and average wind velocity. The configuration of source and sensors is shown in figure 1. Please note that there were sensors in the left half plane of the source as well. However, because the mean wind heading was 45.3° the sensors in left half plane didn't record any data. Thus, only the sensors in right half plane are shown.

The number of sensor locations is very limited and compared to temporal domain, the resolution of data in spatial domain is very low. However, since we want this evaluation to reflect the true performance of classification module only, we do not extrapolate the spatial domain data that would introduce additional approximation errors. For the temporal domain, we take advantage of the availability of data at high resolution and therefore choose the window size of 1 second. Thus, we perform the kalman filter iteration and obtain an updated estimate of transition matrix at each second.

4.1.2 Performance Metric

In this section we provide some metrics to quantify the performance. Since our end goal is classification of regions into safe and danger zones, we can represent the misclassification error by percentage False Negatives and Flase Positives. If the discretized spatial region is represented by N points, and Ω_n and Ω_p represent the set of locations with dangerous and safe level of concentrations respectively. We label the dangerous zones as 1 and safe regions as 0 and represent the true label and estimated label vectors by u^t and u^e respectively. Then the % false negative and % false positive error is given by,

$$\%FN = \frac{1}{|\Omega_n|} \sum_{i, i \in \Omega_n} |u_i^t - u_i^e| * 100 \tag{16}$$

$$\%FP = \frac{1}{|\Omega_p|} \sum_{i, i \in \Omega_p} |u_i^t - u_i^e| * 100 \tag{17}$$

In addition to the binary classification error, quantification of actual error in concentration values is also important. For that purpose, normalized eucledian norm of the error vector is a common metric, However, the 2-norm error overshoots when the actual concentration values are very small (close to zero) and the estimated values are also very small but still many times of the true values. Thus, the 2-norm metric is unable to discriminate between the cases when the concentration values and the error is actually significant and when the true values are just too small. In order to take care of this tendency of concentration map to become extremely sparse and small in magnitude, we use the log error metric,

$$Log\ Error = \frac{\sqrt{\sum_{i=1}^{N} [log(c_i^e) - log(c_i^t)]^2}}{\sqrt{\sum_{i=1}^{N} [log(c_i^t) + \epsilon]^2}} \tag{18}$$

Where, c^t and c^e represent the true and estimated concentration map and ϵ is a small term added to ensure that the denominator never equals to zero.

4.1.3 Experiment Design and Setup

The next important step after defining the performance metric is the choice the parameter that is varied. Since we want to evaluate the system performance at unsampled locations utilizing the sampled data, the amount of sampled data is the most suitable candidate to vary. Thus, we evaluate the estimation accuracy against the number of sampling locations. Once a set of sampling locations are chosen, they are kept fixed throughout the trial. Utilizing those selected sensors' data, per second estimates of GDM snapshots are obtained and compared with true maps to compute the % false negative, % false positive and log-error. Finally, the average performace over the entire trial is reported.

At this point, it is important to note that for a given number of sensors, one set of sensor locations can be more ideal than the other in terms of improving estimation accuracy. To account for this, we choose the set of sampling locations randomly and repeat the experiment over multiple trials. At the end, mean performance for these monte carlo runs is computed.

4.1.4 Results and their Analysis

In this subsection, we present the result for evaluating the estimation module against the number of samples.

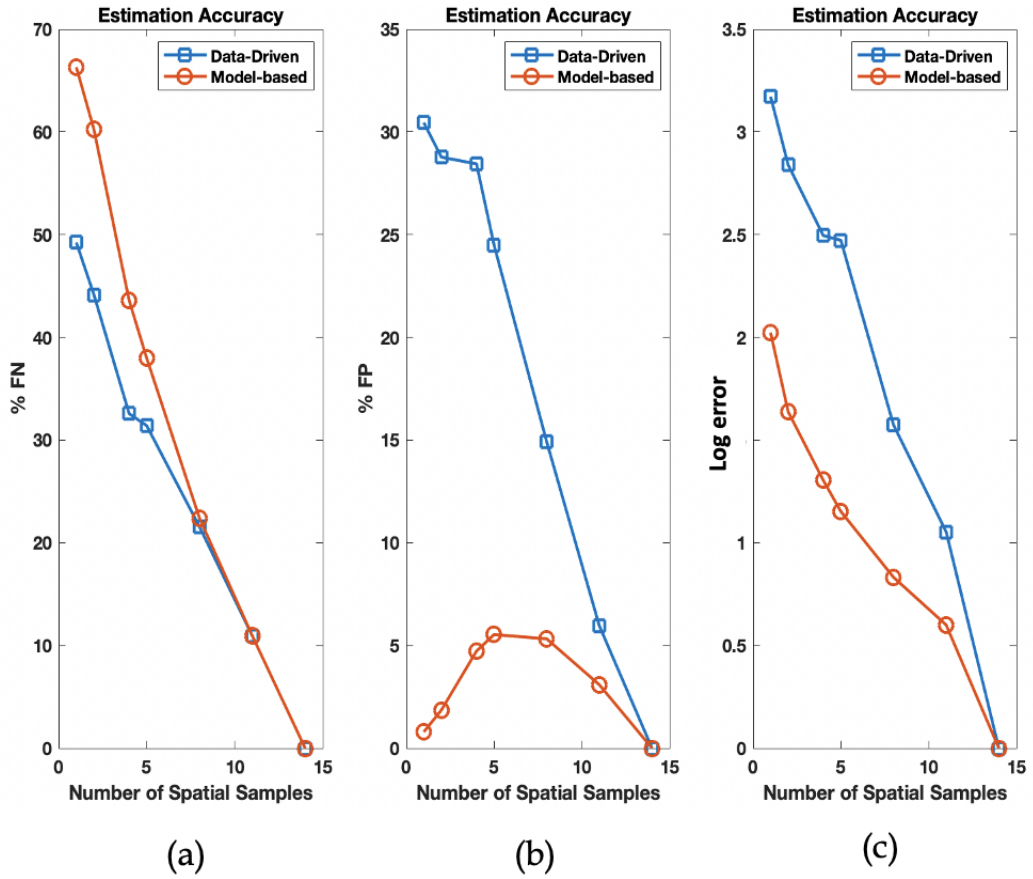

Figure 2: (a) % False Negatives vs. number of samples (b) % False Positives vs. number of samples (c) % Log Error vs. number of samples

Fig. 2(a) shows the decay in % False Negatives as the number of samples are increased from one to fourteen. It can be observed that for extremely small number of samples, the model-based approach has a significantly higher false negative rate compared to the data-driven approach. The improvement of purely data-driven approach over the model-based can be explained by the advantage that data-driven method has because of larger initial overhead. It was explained earlier that to get the first estimate of tranisition matrix, the data driven method needs atleast N equispaced data samples in time compared to only two samples required by the model-based approach. When the number of spatial locations being sampled are extremely small, this initial overhead provides a significant amount of more information to data-driven approach compared to the model-based one. Thus, we observe that when number of spatial samples are small, the data-driven method has better performance than model-based. However, as the number of spatial samples increases, the false negative rate for model-based method approaches that of a data-driven method.

Fig. 2(b) shows the False positive performance against the number of spatial samples for

both methods. First of all, the model-based method shows a sharp decay when the number of samples exceed five. This helps us classify the sampling locations into three subsets. The first subset ranges between 1-5 with high misclassification rate and a gentle slope showing little improvement with increasing samples. The second subset contains samples between 5-10. This region has moderate error rate and has steep slope showing significantl improvements. The third region is basically when high amount of information is being sampled and only a little is to be estimated. It is natural that the error rate is extremely low in this region and we observe a decay with increasing samples for both model-based and data driven approach. Although, both approaches follow the intuition in third subset, we do not observe a decaying trend in model-based approach. It can be seen that with moderate number of samples, the model-based appraoch has a tendency to overestimate concentration values resulting in increasing false positives. This can be explained by the fact that model-based appraoch extrapolates the data in space through diffusion and wind. Since, we are using only average wind velocity and do not take into account the variations in wind field, the model-based approach can overestimate the transport of contaminant through advection and diffusion to certain spatial regions. This is where we see the impact of bias introduced by the use of transport equation. However, it is important to note that even with this tendency to overestimate concentration values, the model-based appraoch has significantly lower false positive rate than the purely data-driven method.

Finally we have the log-error in Fig. 2(c) from which we can observe that it captures the combined effect of both false negative and false positive error rates. The division of decaying rate into three categories according to the number of samples is observed in the log-error plot as well. Furthermore, compared to the purely data-driven method, the model-based approach has a significantly smaller error.

Findings : Going back to the research questions we posed earlier, we briefly state our findings.

- Firstly the misclassification accuracy is very high in the first subset of samples that range between 1-5 samples. However, we observe significant improvement and a sharp decay in error as the sampling locations exceed five.

- A comparison between two approaches show that even with negligible initial overhead model-based approach results in an overall lower average misclassification error compared to purely data-driven approach. The main reason is that data-driven method lacks the ability to extrapolate information in spatial domain that is possessed by the model-based approach which leverages the advection and diffusion transport phenomenon.

- The integration of transport equation in model-based approach does introduce a bias that results in an increasing false positive rate with increasing samples. However, even after this tendency to slight overestimate, the compromise in performance is below 5% and the false positive rate of model-based approach is still much lower than that of purely data-driven method.

4.1.5 Achievable Estimation Accuracy

Issue In the previous subsection, we observed the impact of number of sampling locations on the average estimation accuracy. However, in addition to the number, the choice of sampling locations for a given number can also have an impact. Since, the previous result averaged estimation accuracy over multiple randomly chosen locations, we were unable to observe how and if one set of locations is better than the other. Research Question Thus, it is important to investigate how the impact of the choice of locations vary as the number of sampling locations are varied. It is also going to be particularly helpful in identifying the bounds on achievable estimation accuracy. While it was shown in the previous section that the average performance of model-based approach is better than the data-driven approach, the same can not be said about the highest achievable accuracy. Hence, it is important to characterize and compare the evolution of error bounds for both methods as number of samples vary.

Experiment Design The design of this experiment is very similar to the previous except for one major difference. For a given number of spatial samples, we randomly choose the sampling locations and compute the % False Negatives, % False Positives and Log error. We repeat this process multiple times and each time a new set of locations are randomly chosen. However, instead of evaluating the average estimation accuracy over all these trials, we compute the maximum and minimum error metrics. The reason for choosing maximum and minmum values instead of standard deviation or variance is that the maximum and minimum values provide a more clear bound on the performance which is not very easy to see from standard deviation.

Result and Findings The results for this experiment are presented in Fig. 3. Again we have three subplots for each performance metric i.e False Negative, False Positive and Log Error. For a given number of samples, each vertical bar has a dash at its lower and upper end representing the minimum and maximum error respectively while the circle represents the average value.

First of all, we observe from Fig. 3(a) that both the lower and upper bounds on % FN are monotonically decreasing as number of samples increase. Comparing the two approaches, we further observe that the lower bound on error for data driven method is lower than that of model-based method. Moreover, the upper bound for model-based is also higher when number of samples are small. However, as the samples increase the upper bound of data-driven method exceed the model-based implying that it is better to use model-based approach with moderate-to-high number of samples when a guaranteed reliability is a key factor. Furthermore, we observe that the trend is completely reversed when we look at % FP in Fig. 3(b). Model-based approach has an achievable false positive rate of almost zero percent whereas the achievable lower bound of the same error for data-driven method is much higher and therefore when we observe the combined effect of Fig 3(a) and 3(b) in 3(c), we observe that the achievable lower bound error of model-based method is much lower than that of data-driven approach. Moreover, the upper bound for model-based error is also always much lower than that of data-driven approach. This makes model-based approach even more reliable when a guarantee on maximum error is required.

Another important aspect of these plots is the length of vertical bars. They quantify

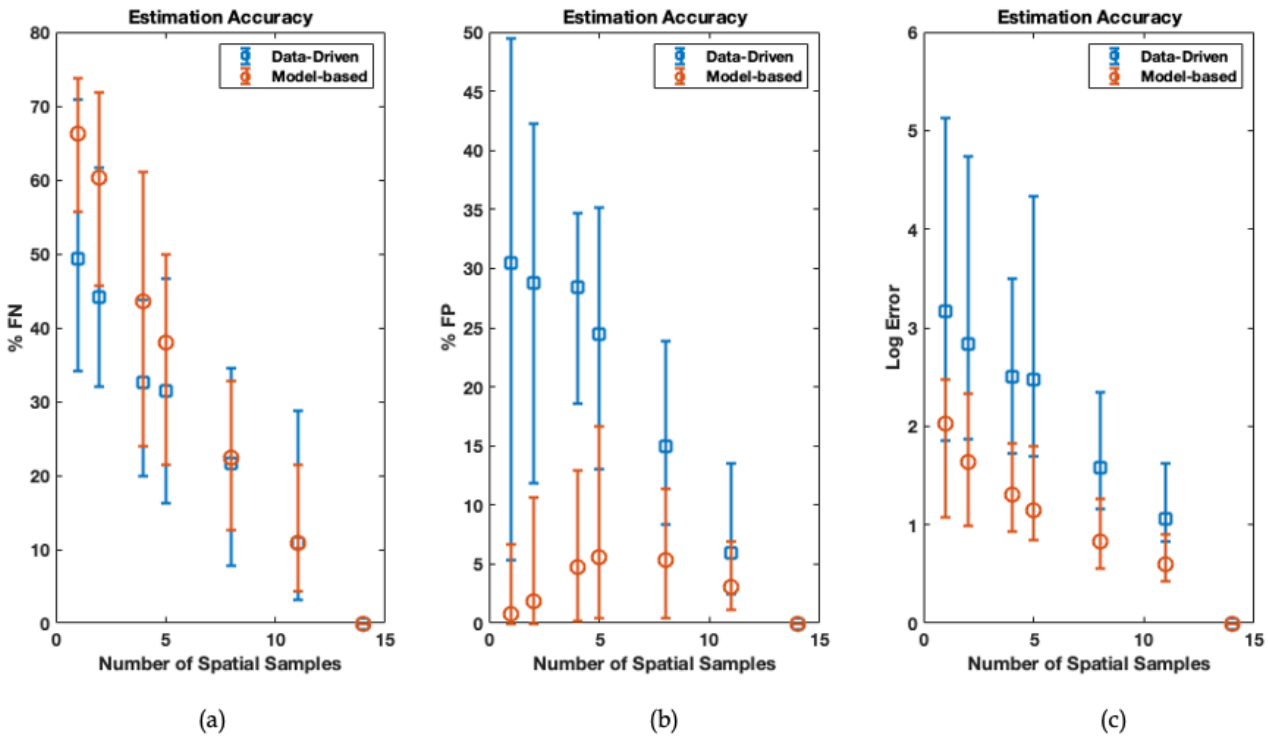

Figure 3: Deviation in Estimation Accuracy

the impact of choice of locations. First of all, we observe that the lengths of bars are very significant showing how careful choice of locations can improve the performance. Also the vertical length or variation is not always decreasing as number of samples increase. Thus, not only flight planning is important when the resources are very limited and only a small number of samples can be collected but also when we have enough resources to sample moderate to high number of spatial locations. This also signifies that random sampling is inherently an unreliable method as there is a high tendency to lose a significant improvement in error performance that could be achieved otherwise.

Secondly, it should be noted that the the length of blue bars are almost always longer than corresponding orange bars. This implies that variation resulting from different choices of locations is much more significant in data-driven method than in model-based approach which can be explained by the transition matrix models derived in (5) and (12). The model-based transition matrix (12) integrates advection and diffusion that allows it to extrapolate concentration values from meausred locations to other unsampled locations which is missing in purely data-based transition matrix (5). This ability to spatially extrapolate the data using the naturally present dispersion mechanism somewhat accommodates for a different choice of sampling locations. Since, it is solely the measurements based on which (5) constructs A, the impact of different set of locations is also much more significant. This encourages us to further conduct a deeper analysis of the transition matrix itself which is provided in the next section.

4.2 Transition Matrix Accuracy

Issue The output of the estimation and prediction module is evaluated through false negatives, false positives and log error in the previous sections. However, those output results strongly depend on the key element of this module which is the transition matrix. Transition matrix is the hidden auxiliary variable inside the system black box that we have tried to estimate through a purely data-driven and a model-based approach. While, the output performance is a key metric to evaluate how good the proposed system is, it is critical to evaluate how accurate the transition matrix estimate is to explain the evolution of that matrix. Research Question Thus, it is important to quantify the relation between transition matrix accuracy and the available spatial information. Furthermore, a comparison between model-based and data-driven approach is needed to validate the conclusions we drew in previous section that favored model-based method over the other.

Experiment Design In order to evaluate the accuracy of transition matrix, there are two main design aspects. The first issue arises from the lack of availability of *true* transition matrix. Since, the transition matrix is the variable inside the black box and from (2) it is clear that we can only measure the raw concentration values, it is not possible to experimentally measure the transition matrix values directly.

To address this issue, we exploit the results in Fig. 2 and 3 to define a *relative true* transition matrix. While we don't have any means to measure the true transition matrix, we can define a notion of *good* and *bad* transition matrices by using the estimation accuracy results. It can be observed from Fig. 2 and 3 that when all the available fourteen spatial locations are sampled, the resulting estimation error is zero. This happen when we exploit all the available spatial information and there is essentially nothing to estimate in the current GDM snapshot. We can treat the transition matrix associated with this scenario as the best estimate of transition matrix and call it A_t. This best A_t learned from a *complete* set of information can act as a benchmark for other transition matrices learned from *partial* spatial information.

The second design aspect is defining a metric to compare the estimated A_e to the benchmark A_t and define the accuracy. Since, error-norm is a good reference to compare two vectors and matrix is just a set of vectors, a normed error can provide us an overall insight into how close the estimated A is to the benchmark. Hence, we use the forbenius norm of error matrix that provides a point-by-point comparison between matrix enteries and normalize it with the norm of the benchmark,

$$Err_N = \frac{||A_t - A_e||_F}{||A_t||_F} \tag{19}$$

where the Forbenius norm of an $N \times N$ matrix A is given by,

$$||A||_F = \sqrt{\sum_{i=1}^{N}\sum_{j=1}^{N} |A_{i,j}|^2}$$

where the subscript represents the row and column respectively.

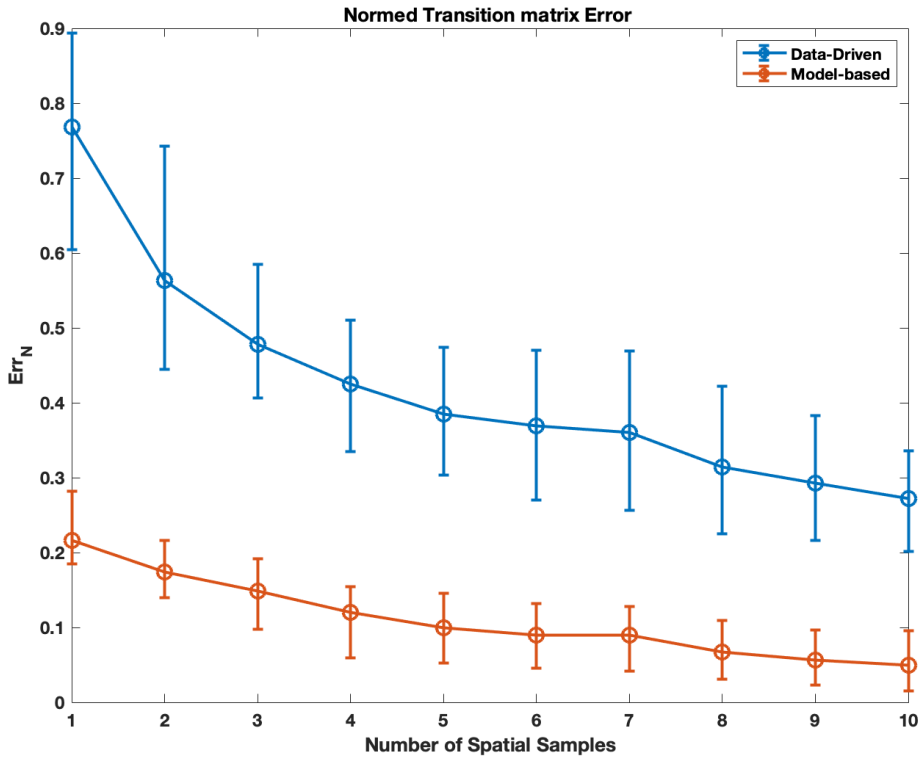

Figure 4: Normalized Forbenius-norm Error

Since the evaluation parameter is the same i.e the the number of spatial samples, we still choose them randomly and run the experiment multiple times. During each run, the transition matrix is updated at each time iteration and compared to the transition matrix obtained from complete spatial data for that time stamp. At the end of these iterations, the average error is evaluated. The process is repeated multiple times and the average, maximum and minimum errors are reported so they can be compared to the results in previous section.

Result and Findings The Forbenius norm of error matrix is plotted against the number of spatial samples in Fig. 4. The upper and lower dashes of the vertical bars represent the maximum and minimum error respectively, while the circles represent the mean error.

Firstly, if the mean error performance is compared to the mean estimation log-error in Fig. 2(c), we can observe that the just like the estimation error, the transition matrix error also decreases monotonically with increasing number of samples. Thus, it validates that the transition matrix accuracy maps directly into the output estimation performance. The drop in error with each increasing sample location is much higher in data-driven method compared to model-based approach which affirms extreme dependency of data-driven approach on the actual measurements.

Secondly, it is worthwhile to compare the vertical bars with the bounds and variation trends shown in Fig. 3(c). The length of blue bars is longer than the corresponding orange bars in both plots. This again corroborates the fact that compared to model-based approach, data-driven method is more prone to degradation in performance from a bad choice of sensors. The fact that the length of bars is not decreasing as number of samples increase,

highlight that careful adaptive sampling is equally important with larger available locations as with a smaller number. It is also important to note that an overall higher error in data-driven A reflects its tendency to overestimate the values which is also seen from the false positive results earlier.

Issue Although the norm of the actual error between two matrices give us an insight into how accurate an estimate of transition matrix is, it can be argued that the optimum transition matrix A might not be unique. Consider the expansion of first row of (1),

$$c_1[n+1] = A_{1,1} * c_1[n] + A_{1,2} * c_2[n] + A_{1,3} * c_3[n] + ... + A_{1,N} * c_N[n] \tag{20}$$

The concentration map at time n is being multiplied by coefficients in A to get the map at time $[n+1]$. Now there can be several possibilities for these coefficients to get the same $c_1[n+1]$. For instance it can be simple scaling of previous concentration value at the same point through $A_{1,1}$ or a combination of other concentration values. Thus, an absolute difference between two matrices might not perfectly reveal how 'similar' they are in their effect. Research Question Hence, it is important to conduct an evaluation of transition matrix accuracy based on its structure and its impact it creates when used in a state-space formulation (1) rather than its absolute values.

Experiment Design The state-space formulation provided in (1) shows that A is simply a transformation on the the gas distribution map that maps it to the column space of A. There can be several matrices that could have different entries but result in similar transformation. Thus, we need a characterization of similarity between two matrices. Now, we take a look at the definition of similar matrices. Two matrices A and B are similar if there exists an invertible P such that,

$$A = P^{-1}BP \tag{21}$$

One major and useful property of similar matrices is that they have exactly same eigenvalues. Please note that eigenvalues are also called the *spectrum* of a matrix operator More details can be added about spectrum theorem to convey the message that eigenvalues are a useful tool for matrix characterization. Thus, we can quantify the similarity between the transformation of estimated transition matrix A_e and our best estimate A_t through the eigenvalues. Since trace of a matrix is the sum of its eigenvalues, we evaluate the trace of error matrix and normalize it with the trace of A_t,

$$Trace_N = \frac{trace(A_t - A_e)}{trace(A_t)} \tag{22}$$

where,

$$trace(A) = \sum_{i=1}^{N} A_{i,i}$$

Please note that since the trace is the sum of diagonal elements it also gives us an intuition of the new concentration values at a certain location depends on the previous value at the same location.

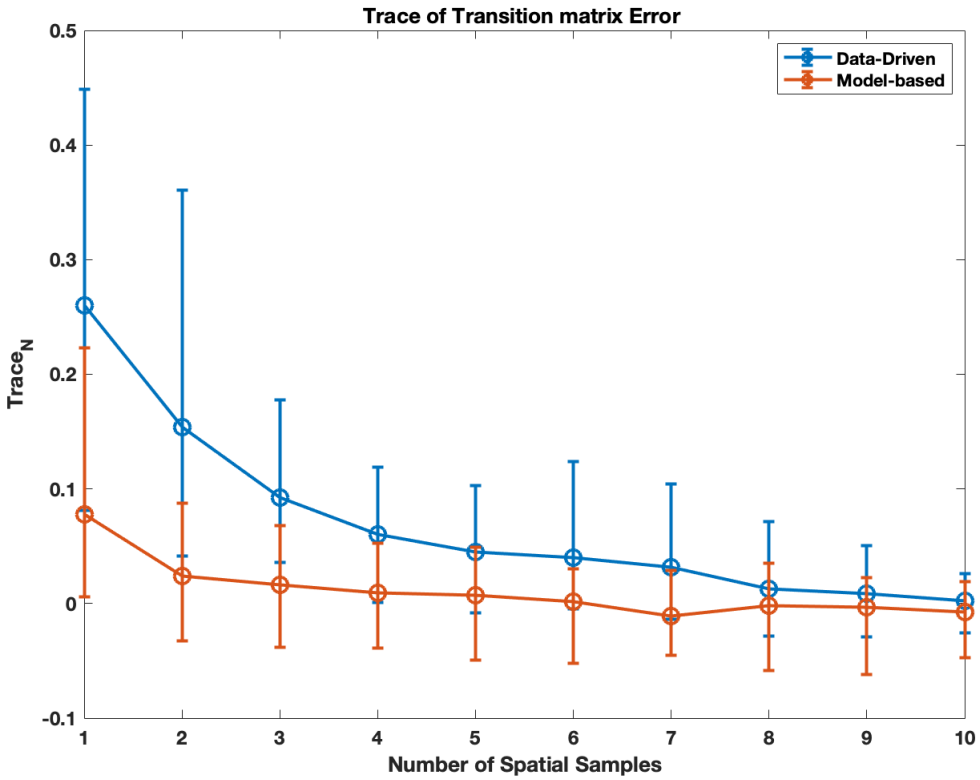

Figure 5: Normalized Trace Error vs. Number of Spatial Samples

Result and Findings We present the normalized trace of error transition matrix in Fig.5. Like the previous plots, the average, maximum and minimum error is reported and the number of samples are varied across the x-axis.

First of all, the monotonically decreasing error with increasing number of samples is evident from this plot as well. We observe that this improvement is more significant for the data-driven method. This corroborates our previous findings. However, there are two more interesting observations. Firstly, we observe that the the lower dashes of the bar that correspond to the minimum error are becoming negative. The negative values correspond to scenarios when estimated diagonal entries of A_e are larger than those of benchmark A. This implies that the concentration map is being overestimated resulting in higher false positives. This is contrary to all our previous results where the data-driven always had much higher false positives than the model-based approach. The second observation is about the decrease in length of blue bars as number of spatial samples increase. Again this was not observed in the previous results.

Issue Both of these observations stem from one main problem associated with the trace of the matrix. The trace provides a collective sum of *all* eigenvalues or the diagonal entries. Thus, there is a high possibility that only a few slightly eigenvalues have negative errors that dominate the entire trace value. Research Question Thus, in order to exploit the true similarity between estimated and benchmark transition matrix, it is important to analyze

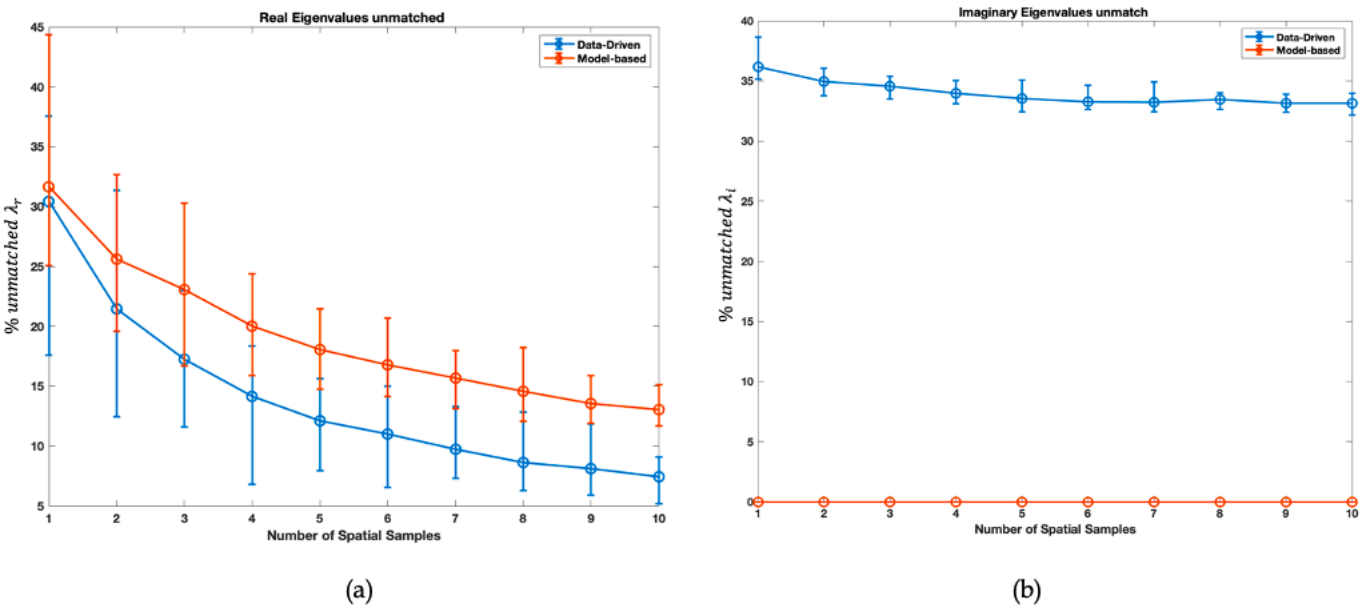

Figure 6: Uncaptured spectrum by estimated transition matrix

the individual eigenvalues instead of a complete sum.

Experiment Design As mentioned earlier, the eigenvalues of two similar matrices are exactly the same. However, as observed from non-zero error in Fig.5, even for high spatial samples thats not the case. To resolve this issue, we first set a small margin ϵ and if the two eigenvalues are within ϵ-proximity of each other, we consider them to be same. Secondly, after computing the eigenvalues λ^t and λ^e of benchmark A_t and estimated A_e, we perform a matching function. The idea of matching is that the eigenvalue pairs are created such that each pair is within ϵ-proximity. This allows us to observe what eigenvalues or eigenmodes of benchmark matrix A_t appeared in the estimated A_e. Since, the eigenvalues are complex, we match the real and imaginary part separately. Finally, we compute the percentage of eigenvalues that did not appear in the estimated transition matrix,

$$\%\ \ unmatched\ \ \lambda = \frac{|U|}{|V|} \tag{23}$$

where the set V contains the eigenvalues of A_t and the set U contains the set of unmatched eigenvalues of A_t. Since eigenvalues are called the spectrum of a matrix operator, we can intuitively visualize this metric as a quantification of spectrum not captured by the estimated transition matrix.

Results and Findings The percentage unmatched real and imaginary eigenvalues are presented in Fig.6(a) and Fig.6(b) respectively. We can observe that the % of unmatched eigenvalues in model-based approach is higher than data driven method. Whereas, for the imaginary part, the all 100% values are match in the model-based approach. Although, if

we take a combined look at both of them, it would result in a lower collective unmatching for model-based approach. However, individually these results do reflect the trend observed in false negatives and false positives rate. From the previous findings, we observed that model-based approach provided a high false negative, a much lower false positive rate and an overall lower log-error rate when compared to data-driven approach. The trend for false negatives iand dalse positives s close to that of unmatched real eigen values in Fig.6(a) and imaginary eigenvalues in Fig.6(b) respectively. However, it is hard to explain this connection or believe that its true unless a physical explanation of the real and complex eigenvalues is defined.

References

[1] N. R. Council, *Tracking and Predicting the Atmospheric Dispersion of Hazardous Material Releases: Implications for Homeland Security*. Washington, DC: The National Academies Press, 2003. [Online]. Available: https://www.nap.edu/catalog/10716/tracking-and-predicting-the-atmospheric-dispersion-of-hazardous-material-releases

[2] Y. Hua and T. K. Sarkar, "Matrix pencil method for estimating parameters of exponentially damped/undamped sinusoids in noise," *IEEE Transactions on Acoustics, Speech, and Signal Processing*, vol. 38, no. 5, pp. 814–824, 1990.

[3] D. Logan, *First Course in the Finite Element Method*. Thomson, 2007. [Online]. Available: https://books.google.com/books?id=wjr3ArdvAc4C

MORE TO ADD

- A figure explaining the scenario in Section 1
- More details on estimating noise covariances
- A figure giving a visualization of elements and nodes in FEM
- A figure of the actual plume generated from FEM in Section 3.2
- References for transport PDE, FEM,